FDTD Method with a Conformal Polygonal Mesh and Perfectly Matched Layer Absorbing Boundary Condition

Krishna Naishadham and Zhian Lin

Department of Electrical Engineering
Wright State University, Dayton, OH 45435

Abstract: The accuracy of the finite–difference time–domain (FDTD) method in microwave circuit simulation depends significantly on the accuracy with which the computational grid resolves the structure's geometry, especially when it has curved boundaries (*e.g.*, dielectric resonator filters). Body–conformal grids allow for accurate resolution of the object, but complicate the implementation of absorbing boundary conditions (ABC). In order to address this conflict, we propose a new FDTD implementation in which triangular grids are used near the scatterer boundary, while rectangular grids are employed away from the scatterer to facilitate simple ABC. The improvement in accuracy by the new method is illustrated by its application to the scattering from a circular dielectric cylinder.

1. Introduction

The FDTD method involves numerical approximation of the Maxwell's equations inside a discretized computational volume using centered finite differences. The discretization grids are usually rectangular in shape, but triangular [1] two–dimensional (2–D) grids, polyhedral 3–D grids [2], and polygonal prisms [3] have also been employed in certain problems. The proper choice of the grid should enable accurate geometrical modeling of arbitrarily shaped circuits or scatterers used in microwave systems. In particular, a rectangular mesh introduces stair-casing errors for curved object boundaries, sometimes forcing excessive number of cells to be employed for adequate resolution of the geometry. Obviously, this is not an efficient solution.

A second problem in modeling geometries of arbitrary complexity is the requirement that the discretization scheme also model the absorbing boundary accurately. While a conformal mesh may be useful to accurately model the scatterer boundary, it may not be needed at the location of the absorbing boundary. For example, some researchers have employed generalized non-orthogonal grids that conform to the curved object boundaries [4], [5], but, these analyses have been primarily confined to perfectly conducting scatterers or waveguiding problems. The reason for this limitation is perhaps the difficulty in implementation of a good ABC in such a coordinate system. However, this limitation can be overcome by employing a local polygonal mesh around the scatterer, and gradually replacing the polygons with rectangular cells away from the scatterer, so that simple ABCs, which have been exclusively developed for rectangular meshes, can be employed. Besides improving the accuracy in resolving local features of the scattering object, such an implementation preserves the simplicity of rectangular mesh modeling at the absorbing boundary. In this paper, we report the formulation and implementation of such an approach, and demonstrate significant improvement in accuracy. The proposed method differs substantially from existing conformal FDTD methods for modeling microwave circuits (*cf.* [3]), because the conformal mesh is employed only in a small region encompassing the circuit or the scatterer. Therefore, the proposed contribution is anticipated to improve the computational efficiency and ease of implementation of the conformal FDTD method.

The new conformal FDTD method is applied to simulate the electromagnetic (EM) scattering from a circular dielectric cylinder. For simplicity, a 2–D geometry which has a closed-form analytical solution is chosen for testing the algorithm. The perfectly matched layer (PML) absorbing boundary condition for an orthogonal coordinate system [6] is used, since it can absorb multi-directional incident waves propagating away from the polygonal model of the scatterer.

2. Methodology

In the finite-difference time-domain algorithm, the discrete approximations for the EM field can be derived from the integral form of Maxwell's equations. A triangular tessellation consisting of a primary grid with axial electric field located at the triangle vertices, and tangential magnetic field located along a secondary grid passing through the centroids of adjacent triangles, is employed (see Fig. 1). The pertinent cylindrical coordinate system is defined in Fig. 2, where the unit vectors $\hat{s}$ and $\hat{n}$ are tangential and normal, respectively, at an arbitrary point on a surface contour such

0-7803-4603-6/97/$5.00 (c) IEEE

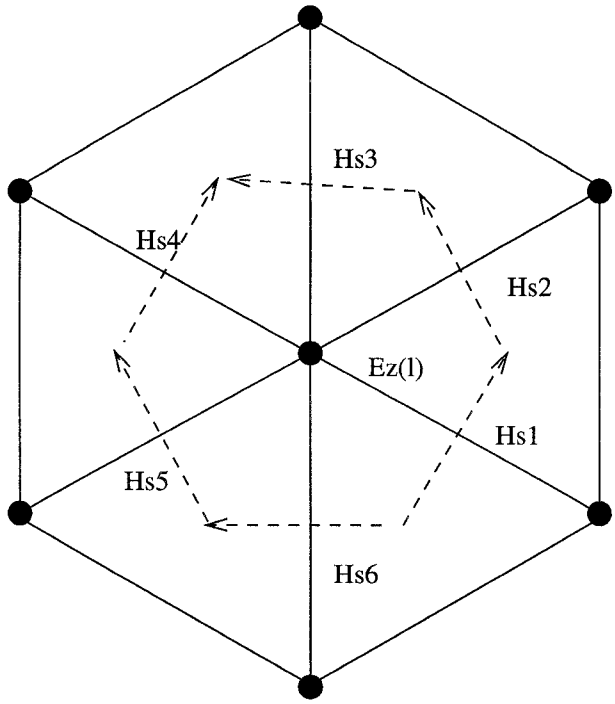

Figure 1: Unit cell with E–nodes at triangle vertices and H–nodes at the edges of a hexagonal contour.

that $\hat{n} \times \hat{s} = \hat{z}$.

We restrict attention to a 2-D transverse magnetic (TM) problem with the electric field $\vec{E} = \hat{z}E_z$, and the magnetic field $\vec{H} = \hat{s}H_s + \hat{n}H_n$, which satisfy the Maxwell's equations:

$$\nabla_T \times \eta_0(\hat{n}H_n + \hat{s}H_s) = \eta_0\sigma_e E_z + \hat{z}\epsilon_r \frac{\partial E_z}{c\partial t} \quad (1)$$

$$\frac{\partial E_z}{\partial n} = \sigma_m H_s + \mu_r \eta_0 \frac{\partial H_s}{c\partial t} \quad (2)$$

$$\frac{\partial E_z}{\partial s} = \sigma_m H_n + \mu_r \eta_0 \frac{\partial H_n}{c\partial t} \quad (3)$$

In the above, E_z, H_n and H_s are total field quantities, ϵ_r, μ_r, σ_e, σ_m, η_0, and c denote, respectively, relative permittivity, relative permeability, electric conductivity, magnetic conductivity, free space impedance, and speed of light in free space.

It is evident from Fig. 1 that the edges of the secondary grid (hexagons) are perpendicular bisectors of the corresponding triangular edge. Therefore, the polygonal tessellations of the secondary grid are orthogonal to the primary triangular grid. This orthognality leads to decoupling H_n from the field equations as shown next. Applying Stokes's theorem to (1) around the hexagonal contour shown in Fig. 1, since the magnetic field is entirely tangential to the contour, we obtain

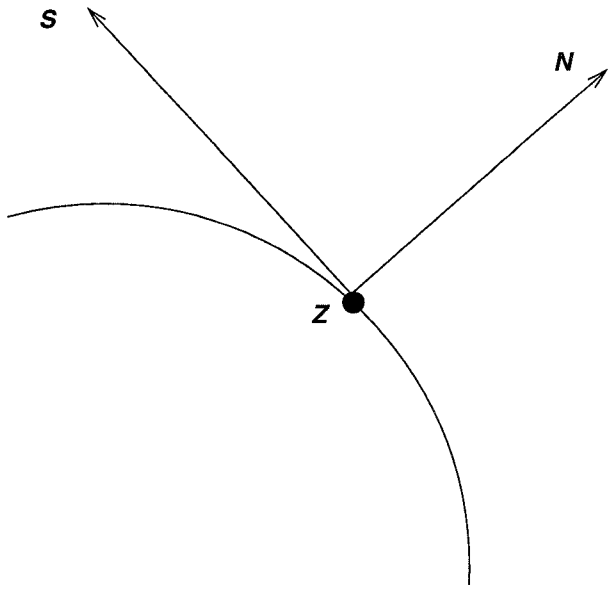

Figure 2: Cylindrical coordinate system.

$$\oint_C \eta_0 H_s \, ds = \int\int (\eta_0\sigma_e E_z + \epsilon_r \frac{\partial E_z}{c\partial t}) \, dA \quad (4)$$

Since H_n is decoupled, (3) can be discarded in the computation. Then, eqs. (2) and (4) provide the update equations for the electric and magnetic fields, respectively. In order to discretize these equations, E_z is computed at the triangular nodes and H_s nodes are centrally located along the hexagonal edges (Fig. 1). An unique orientation is assigned to each H_s, which is counter–clockwise with respect to the edges 1, 2 and 3, and clockwise with respect to the edges 4, 5 and 6.

The discretized finite difference forms of (4) and (2) are given by, respectively,

$$\sum_{k=1}^{M} \eta_0 H^{n-\frac{1}{2}}_{s[k,j]} l_{[k,j]} = \frac{\eta_0\sigma_e A_j}{2}\left[E^n_{z[j]} + E^{n-1}_{z[j]}\right] + \frac{\epsilon_r A_j}{c\Delta t}\left[E^n_{z[j]} - E^{n-1}_{z[j]}\right] \quad (5)$$

$$\frac{1}{d_{[k,j]}}\left[E^n_{z[k]} - E^n_{z[j]}\right] = \frac{\sigma_m}{2}\left[H^{n+\frac{1}{2}}_{s[k,j]} + H^{n-\frac{1}{2}}_{s[k,j]}\right] + \frac{\mu_r\eta_0}{c\Delta t}\left[H^{n+\frac{1}{2}}_{s[k,j]} - H^{n-\frac{1}{2}}_{s[k,j]}\right] \quad (6)$$

where A_j is the area enclosed by the hexagonal contour

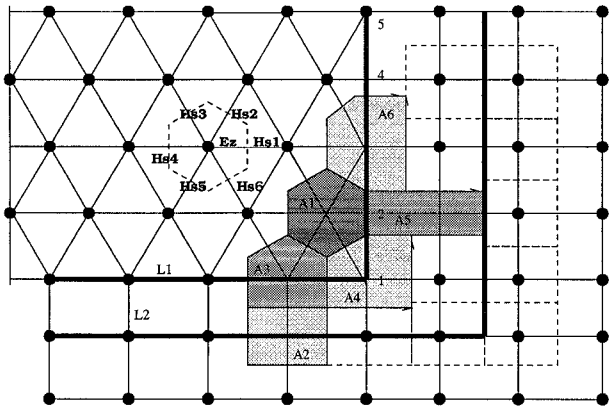

Figure 3: Transition between triangular and rectangular grids.

centered at electric node j, $l_{[k,j]}$ is the length of the k-th hexagonal edge circumscribing node j, and $d_{[k,j]}$ is the distance between electric nodes j and k (see Fig. 1). After re-arranging these two equations, we obtain the iterative equations to update the electric and magnetic fields on a triangular grid:

$$E^n_{z[j]} = \frac{C_2 - C_1}{C_2 + C_1} E^{n-1}_{z[j]} + \frac{1}{C_2 + C_1} \sum_{k=1}^{M} \eta_0 H^{n-\frac{1}{2}}_{s[k,j]} l_{[k,j]} \quad (7)$$

$$H^{n+\frac{1}{2}}_{s[k,j]} = \frac{D_2 - D_1}{D_2 + D_1} H^{n-\frac{1}{2}}_{s[k,j]} + \frac{1}{d_{[k,j]}(D_2 + D_1)} \times \left[E^n_{z[k]} - E^n_{z[j]} \right] \quad (8)$$

where $C_1 = \frac{\eta_0 \sigma_e A_j}{2}$, $C_2 = \frac{\epsilon_r A_j}{c\Delta t}$, $D_1 = \frac{\sigma_m}{2}$, and $D_2 = \frac{\mu_r \eta_0}{c\Delta t}$.

Next, we address the modification of these update equations at the transition between triangular and rectangular cells. In Fig. 3, we show the connection cells at the right–bottom corner of the transition region bounded by the two solid lines. For simplicity, we assume equilateral triangles of the same size (each of side $L1$). All polygonal (hexagonal) cells completely inside the connection boundary have the area $A1 = \sqrt{3}L1^2/2$. All rectangular cells outside this boundary have the area $A2 = L1 \times L2$. All transition polygons in the bottom connection region have an area $A3 = (A1 + A2)/2$, except the corner polygon, which has area $A4 = A1/4 + 7A2/8$. The right–side connection cells are divided into odd and even layers, corresponding to node numbers marked as $1, 2, 3 \cdots$ on the right–side boundary. The area of even–layer connection cells equals $A5 = A2$, while that of odd–layer cells equals $A6 = A1/2 + 2A2/3$, with the exception of the corner cell of area $A4$. Because of symmetry, the left–side transition region is treated same as the right–side, and the top region is treated same as the bottom. We then apply the same iterative updates as in eqs. (7) and (8) for the connection cells in the transition region, with the appropriate areas substituted for A_j. Outside the connection region, the fields are updated with the traditional Yee leap-frog algorithm for rectangular cells. The stability criterion is satisfied if we choose the time increment such that

$$\Delta t \leq \sqrt{\frac{2}{3}} \frac{h}{c} \quad (9)$$

where h is the altitude of an equilateral triangle [1].

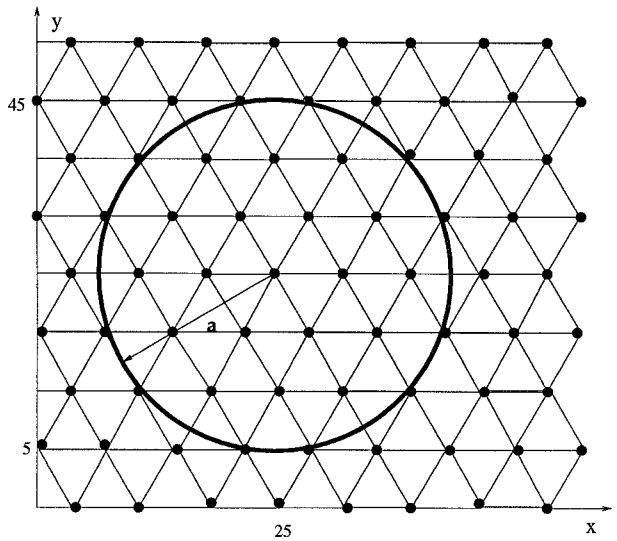

Figure 4: Modeling of a dielectric cylinder with triangular grid. $\epsilon_r = 4$, $\sigma_d = 0$, $a = \lambda_d$.

3. Numerical Validation

In order to validate the afore–mentioned methodology, we consider the scattering by a uniform, circular, dielectric cylinder, assumed to be infinite in z–direction (see Fig. 4). The incident field is a sinusoidal plane wave traveling along y–direction, of the form

$$E^n_z(i, 2) = 1000 \sin(2\pi f n \Delta t). \quad (10)$$

The frequency of the incident wave is 2.5 GHz, and Δt equals 5 ps. The spatial increment $\Delta x = L1 = 0.3$ cm, and $\Delta y = L2 = 0.2598$ cm. Illuminated by such a TM plane wave, the scattering may be considered as 2–D, with only E_z and H_s present in triangular grids, while E_z, H_x and H_y are present in rectangular grids. The PML ABC is used on the outermost rectangular grid of 16 cells thickness [6].

Since the radius of the cylinder equals half the free space

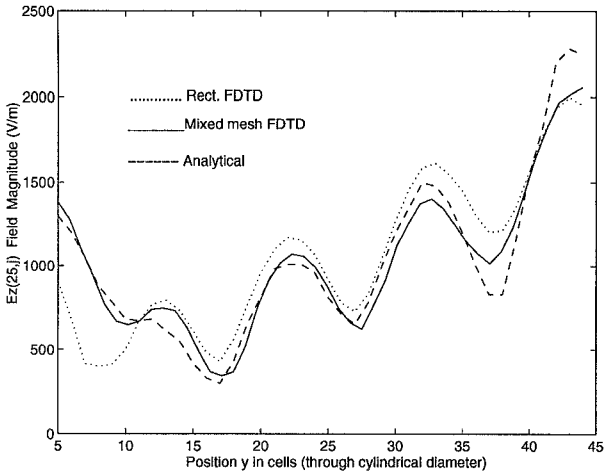

Figure 5: Scattering computation for the dielectric cylinder: dotted line denotes rectangular Yee cell implementation [7], dashed line denotes the mixed polygonal FDTD, and solid line denotes the eigenfunction solution (reference).

wavelength, in one wave cycle (period) requiring 80 time steps, the wave travels from the launching point on the cylinder to the center and back. The computed results are detailed in Fig. 5, which graphs the envelope of $E_z(25, j)$, when the time step n is such that $460 \leq n \leq 500 = n_{max}$. The same geometry and time–window have been used by Taflove and Brodwin [7] for the FDTD simulation with rectangular cells, which requires stair–casing of the cylinder curvature. Fig. 5 shows the improvement caused by the new polygonal FDTD implementation over Taflove's results because of better resolution of the cylindrical boundary. Both the polygonal solution and the traditional Yee implementation are compared with a reference solution computed by eigenfunction summation.

4. Conclusions

We have presented a new conformal FDTD method which utilizes triangular cells to accurately resolve the boundaries of curved objects, and rectangular cells away from the object. The latter facilitates the utilization of a simple ABC such as the PML, exclusively developed for rectangular cells. Field update equations are derived for the triangular cells, and the technique to compute the updates in the transition region between triangular and rectangular cells has been developed. The improvement in accuracy by the new conformal FDTD method in relation to a stair-casing FDTD implementation with rectangular cells has been demonstrated by computation of the plane wave scattering from a circular dielectric cylinder.

Acknowledgement: This research has been partially supported by Avionics Directorate, Wright Laboratory, under Contract F33615-94-C-1424.

References

[1] C. F. Lee, R. T. Shin, and J. A. Kong, "Finite Difference Method for Electromagnetic Scattering Problems," in *PIER 4 Progress in Electromagnetics Research*, New York: Elsevier, pp. 373–442, 1992.

[2] K. S. Yee and J. S. Chen, "Conformal hybrid finite difference time domain and finite volume time domain," *IEEE Trans. Antennas Propagat.*, vol. 42, no. 10, pp. 1450–1455, 1994.

[3] S. D. Gedney, F. S. Lansing, and D. L. Rascoe, "Full–wave analysis of microwave monolithic circuit devices using a generalized Yee algorithm based on an unstructured grid," *IEEE Trans. Microwave Theory Tech.*, vol. MTT–44, pp. 1393-1400, Aug. 1996.

[4] N. K. Madsen and R. W. Ziolkowski, "A three-dimensional modified finite volume technique for Maxwell's equations," *Electromagnetics*, vol. 10, pp. 147-161, 1990.

[5] R. Holland, V. P. Cable, and L. C. Wilson, "Finite-volume time-domain (FVTD) techniques for EM scattering," *IEEE Trans. Electromagn. Compat.*, vol. 33, no. 4, pp. 281–294, 1991.

[6] J.-P. Berenger, "A perfectly matched layer for the absorption of electromagnetic waves," *J. Comp. Phys.*, vol. 114, no. 2, pp. 185-200, Oct. 1994.

[7] A. Taflove and M. E. Brodwin, "Numerical Solution of Steady-State Electromagnetic Scattering Problems Using the Time-Dependent Maxwell's Equations", *IEEE Trans. Microwave Theory Tech.*, vol. MTT-23, pp. 623-630, Aug. 1975.